Structural Analysis of Threonine 342 Mutants of Soybean β-Amylase: Role of a Conformational Change of the Inner Loop in the Catalytic Mechanism[†,‡]

You-Na Kang,[§] Aiko Tanabe, Motoyasu Adachi,[||] Shigeru Utsumi, and Bunzo Mikami*

Laboratory of Food Quality Design and Development, Graduate School of Agriculture, Kyoto University, Uji, Kyoto 611-0011, Japan

Received November 3, 2004; Revised Manuscript Received January 26, 2005

ABSTRACT: Two different conformations of the inner loop (residues 340−346) have been found in the soybean β-amylase structures. In the "product form", the Thr 342 residue creates hydrogen bonds with Glu 186 (catalytic acid) and with the glucose residues at subsites −1 and +1, whereas most of those interactions are lost in the "apo form". To elucidate the relationship between the structural states of the inner loop and the catalytic mechanism, Thr 342 was mutated to Val, Ser, and Ala, respectively, and their crystal structures complexed with maltose were determined together with that of the apo enzyme at 1.27−1.64 Å resolutions. The k_{cat} values of the T342V, T342S, and T342A mutants decreased by 13-, 360-, and 1700-fold, respectively, compared to that of the wild-type enzyme. Whereas the inner loops in the wild-type/maltose and T342V/maltose complexes adopted the product form, those of the T342S/maltose and T342A/maltose complexes showed the apo form. Structural analyses suggested that the side chain of Thr 342 in product form plays an important role in distorting the sugar ring at subsite −1, stabilizing the deprotonated form of Glu 186, and grasping the glucose residue of the remaining substrate at subsite +1. The third hypothesis was proved by the fact that T342V hydrolyzes maltoheptaose following only multichain attack in contrast to multiple attack of the wild-type enzyme.

Glycoside hydrolases (EC 3.2.1.*X*) are enzymes that hydrolyze the glycosidic bonds of polysaccharides by either retention or inversion of the anomeric configuration. They are now classified into at least 94 families based on sequence similarity (*1*, *2*). β-Amylase [α-1,4-glucan maltohydrolase (EC 3.2.1.2)] belonging to glycoside hydrolase family 14 catalyzes the release of β-anomeric maltose from the nonreducing ends of starch, glycogen, and maltooligosaccharides, with inversion of the anomeric configuration (*3*). Mikami et al. first determined the X-ray crystal structures of soybean β-amylase (SBA)[1] complexed with α-cyclodextrin (α-CD) (*4*). Analyses of the maltose and maltal complexes of SBA revealed that two maltose molecules bind in tandem at the active site pocket occupying subsites −2 to +2, where two catalytic residues, Glu 186 and Glu 380, are located between subsites −1 and +1 (*5*, *6*). The recombinant SBA and its crystal structure complexed with β-CD showed almost the same properties and structures as those of the natural SBA (*7*).

Comparison of the apo and maltose-complexed SBA structures has revealed that the most striking differences lay in the two regions involving residues 96−103 (flexible loop) and 340−346 (inner loop). Figure 1a shows the superposition of Cα atoms of the maltose-complexed (PDB code 1BYB, shown in orange) and apo SBA (PDB code 1BYA, shown in green) (*5*). In the wild-type/maltose complex structure, both loop regions move closely toward the maltose molecules upon their binding. The first region is composed of highly conserved ^{96}GGNVGDIV^{103} sequences in β-amylases (Figure 1b). The Val 99 residue, which is located in the middle of the flexible loop, moves about 11 Å upon maltose binding (*4*, *5*). The second region containing residues 340−346 is relatively short. A ^{341}FTC^{343} sequence is located at the active site of SBA and is also highly conserved in β-amylases (Figure 1b). The maximum main-chain movement (2−3 Å) in this region occurs at the Thr 342 residue, which approaches the glucose rings at subsites −1 and +1 by exchanging hydrogen bonds with them.

Pujadas et al. compared the apo enzyme (PDB code 1BYA) with the ligand-bound enzyme structures (PDB codes 1BYB, 1BYC, 1BYD, and 1BTC) of SBA and found that this region adopted two different conformations according to the ligand bindings (*8*). The conformational change upon the ligand binding of this region has also been reported in the structure of apo and maltose-complexed *Bacillus cereus* β-amylase (BCB) (*9*). Kang et al. designated these two

[†] This work was supported in part by a grant of the National Project on Protein Structural and Functional Analyses from the Ministry of Education, Culture, Sports, Science, and Technology of Japan.

[‡] The atomic coordinates and structure factors have been deposited in the Protein Data Bank, Research Collaboratory for Structural Bioinformatics (RCSB), under accession codes 1WDP (apo SBA), 1WDQ (T342V/maltose), 1WDR (T342S/maltose), and 1WDS (T342A/maltose), respectively.

* To whom correspondence should be addressed. Telephone: 81-774-38-3763. Fax: 81-774-38-3764. E-mail: mikami@kais.kyoto-u.ac.jp.

[§] Present address: Baker Laboratory, Department of Chemistry and Chemical Biology, Cornell University, Ithaca, NY 14853-1301.

[||] Present address: Japan Atomic Energy Research Institute (JAERI), Neutron Science Research Center, 2-4, Shirakata-shirane, Tokai, Ibaraki 319-1195, Japan.

[1] Abbreviations: SBA, soybean β-amylase; BCB, *Bacillus cereus* β-amylase; Glc, glucose; α-CD, α-cyclodextrin; β-CD, β-cyclodextrin; G3, maltotriose; G5, maltopentaose; G7, maltoheptaose.

10.1021/bi0476580 CCC: $30.25
Published on Web 03/08/2005

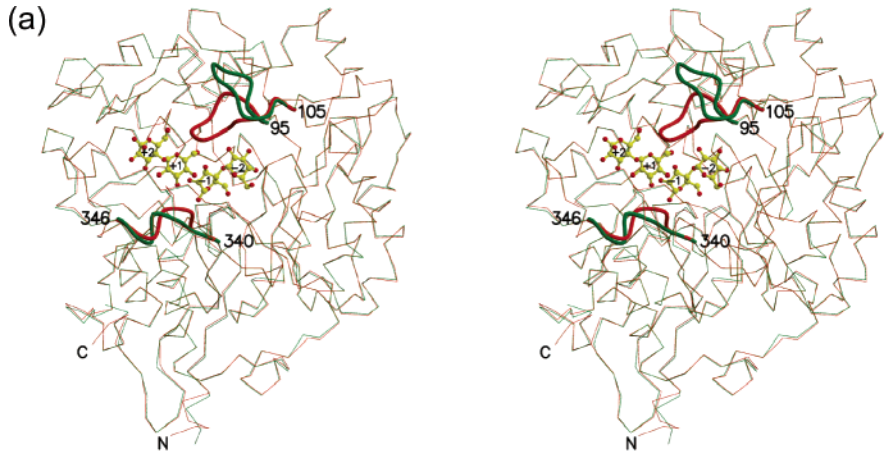

(b)

		*******	** **
P10538	AMYB_SOYBN	CGGNVGDIVNI	NFTCLEM
P10537	AMYB_IPOBA	CGGNVGDAVFI	NFTCLEM
P93594	AMYB_WHEAT	CGGNVGDVVNI	NFTCAEM
P16098	AMYB_HORVU	CGGNVGDAVNI	NFTCAEM
P55005	AMYB_MAIZE	CGGNVGDVVNI	NFTCAEM
P25853	AMYB_ARATH	CGGNVGDIVTI	NFTCLEM
P19584	AMYB_THETU	CGGNVGDTVNI	TFTCLEM
P36924	AMYB_BACCE	CGGNVGDDCNV	TFTCLEM
P06547	AMYB_BACCI	CGGNVGDDCNI	TFTALEM
P21543	AMYB_PAEPO	CGGNVGDDCNI	TFTCLEM
		95 105	340 346

FIGURE 1: (a) Cα superposition of holo (PDB code 1BYB, orange) with apo (PDB code 1BYA, green) SBA in stereo. Maltose molecules are shown in a ball-and-stick model (yellow). The conformational changes are found in two regions (shown in coil representation). The first region is composed of residues 96−103 and the second one of residues 340−346. They are coming close to the maltose molecules in the maltose complex of the SBA structure. (b) Amino acid sequence alignment at two regions of β-amylases from various plants (soybean, P10538; sweet potato, P10537; wheat, P93594; barley, P16098; maize, P55005; *Arabidopsis thaliana*, P25853) and bacterial sources (*Clostridium thermosulfurogenes*, P19584; *B. cereus*, P36924; *Bacillus circulan*, P06547; *Bacillus polymyxa*, P21543). Strictly conserved amino acids are marked with an asterisk. Highly conserved glycine residues in L3 (residues 96−103) endow it with flexibility. Thr 342 in the β6 region (marked in red), which undergoes the largest movement, is strictly conserved in all β-amylases. The multiple sequence alignment was performed using Clustal X (*33*).

different conformations as the "apo form" and the "product form", respectively (*10*). In the product form, the Oγ1 atom of Thr 342 interacted with the O2 of Glu 186 and with the O3 and O4 atoms of Glc(+1), while the Oγ1 atom of Thr 342 created only one hydrogen bond with the O3 atom of Glc(+1) in the apo form (*10*). Although Pujadas et al. suggested that the transition of this region is related to the attachment mechanism of the ligand and thus proposed a "trap trigger" mechanism that made it easier for the ligand to adapt to the active sites (*8*), other structures previously reported, i.e., the wild-type/β-CD complex (PDB code 1BFN) (*7*) and the E186Q/maltopentaose (G5) (PDB code 1V3H) (*10*), also have a conformation identical to that of the apo SBA despite the successful ligand binding, raising a question as to whether the conformational change of the inner loop is induced by the ligand binding during the hydrolysis. Therefore, the precise relationship between the different structural states of this region and their roles in the catalytic mechanism of SBA should be elucidated. In this study, three threonine mutants, T342V, T342S, and T342A, were generated, and their crystal structures in complex with maltose, along with the crystal structure of the apo enzyme, were determined. The results of the kinetic and structural analyses suggested that the movement of the inner loop including Thr 342 plays critical roles in the catalytic mechanism of SBA.

MATERIALS AND METHODS

Site-Directed Mutagenesis and Purification of the Mutant Proteins. The recombinant SBA expression vector (*7*) was used for the construction of Thr 342 mutant plasmids. Site-directed mutagenesis of SBA was performed by using a QuickChange site-directed mutagenesis kit (Stratagene, La Jolla, CA). The wild-type SBA in the pKK233-2 vector was used as a template. The mutants were prepared by PCR using cloned Pfu polymerase (Takara, Japan). Three mutants, T342V, T342S, and T342A, were created. The correct mutations were verified by DNA sequencing. Mutant enzymes were overexpressed in *Escherichia coli* strain JM105 grown at 37 °C in LB medium (and induced at 18 °C) and purified as described for the wild-type enzyme (*7*).

Assay Methods. The kinetic data for the Thr 342 mutant enzymes were determined using potato amylopectin as a substrate at 37 °C in 0.1 M sodium acetate buffer (pH 5.4) containing 1 mM EDTA and 18 mM 2-ME, according to Bernfeld's method (*11*), but with a slight modification (*12*). Substrate concentrations were varied from about 0.1 to 8 times of K_m (0.2−15 mg/mL). One unit was defined as the activity releasing 1 μmol of maltose for 1 min. Enzyme concentrations in the incubation mixtures ranged from 0.5 to 24 μM for the mutant enzymes. The k_{cat} and K_m values were obtained by fitting the initial rate, v, as a function of the substrate concentration using the computer program KaleidaGraph 3.5 (Synergy Software, Reading, PA). Protein amounts of the purified enzymes were determined by an extinction coefficient of 97 $mM^{-1}\cdot cm^{-1}$ at 280 nm (*12*). The ratios of single-chain and multichain attack of wild-type enzyme and T342V were estimated by the method of Nakatani (*13*) by using maltoheptaose (G7) as a substrate.

The amount of substrate and the product (G7, G5, G3, and maltose) during the enzyme reactions was determined by a Shimadzu HPLC system equipped with a Bio-Rad Aminex HPX-42A column, 300 × 7.8 mm, and a Shimadze RID-6A RI detector.

Fluorometric Titration. Fluorescence spectra were measured with a Hitachi F-3000 spectrometer at 25 °C with an excitation wavelength of 282 nm and emission wavelength of 290 nm. Fluorometric titration of Thr 342 mutant enzymes in 0.1 M sodium acetate buffer (pH 5.4) containing 1 mM EDTA and 18 mM 2-ME was performed with maltose (0−56.8 mM) and α-CD (0−3.5 mM), respectively, and the subsequent determinations of the dissociation constant (K_d) and ΔF (%) values were calculated. Kinetic data were fit using the KaleidaGraph 3.5 software package (Synergy Software, Reading, PA).

Crystallization. Purified mutant proteins were crystallized using the hanging-drop vapor diffusion method under the conditions described previously for the crystallization of the wild-type SBA (*7*). The solution in the crystallization drop was prepared on a silanized coverslip by mixing 5 μL of protein solution of 10 mg/mL concentration with 5 μL of reservoir solution containing 40%−50% (w/v) ammonium sulfate, 1 mM EDTA, and 18 mM 2-ME in 0.1 M sodium acetate buffer at pH 5.4. Droplets were equilibrated against 1 mL of the reservoir solution at 4 °C. Prior to data collection, the crystals were soaked gradually in 0.1 M sodium acetate, pH 6.1, containing 50% ammonium sulfate, 1 mM EDTA, 20 mM DTT, 300 mM maltose, and 30% (v/v) glycerol as a cryoprotectant. After performing several capillary experiments, we determined that the results at pH 5.4 (the optimum pH of SBA) corresponded to the freezing experiments at pH 6.1 (unpublished data). After 10−30 min of stepwise incubation in cryosoaking buffer, the crystals were frozen under a cold nitrogen gas stream at 100 K.

Data Collection and Refinement. The crystal data of the T342V/maltose were collected at a resolution of up to 1.12 Å by the rotation method with oscillation angles of 1.0° at the beam line BL41XU of SPring-8 (Hyogo, Japan) using a MAR CCD detector at 100 K. The wavelength of the incident X-ray was 0.71 Å, and the crystal-to-detector distance was 110 mm. For the apo wild-type enzyme and T342S/maltose, the data were collected at respective resolutions of up to 1.25 and 1.35 Å at the same beam line using a Rigaku R-axis V imaging plate detector with a crystal-to-detector distance of 300 mm. The collected images were processed with the HKL2000 program (*14*). The crystal data of the T342A/maltose were collected at a resolution of up to 1.60 Å using Cu Kα radiation ($\lambda = 1.5418$ Å) with a Bruker Hi-Star area detector coupled to a MAC Science M18XHF rotating-anode generator at a temperature of 100 K. The collected data were processed with the SADIE and SAINT software packages (Bruker). Model building was performed using the graphics program TURBO-FRODO (AFB-CNRS, France) on a Silicon Graphics Octane computer. The refinement calculations were carried out with the programs CNS (*15*) for T342A/maltose and SHELXL97 (*16*) for apo, T342V/maltose, and T342S/maltose. The final models of apo, T342V/maltose, and T342S/maltose included *B*-anisotropies and hydrogen atoms. Stereo pictures were created with Molscript (*17*) or Bobscript (*18*) and Raster3D (*19*). The sugar puckering parameters (Φ^2, Θ, Q) were calculated by method of Cremer and Pople (*20*) using a program package of PLATON (*21*).

Table 1: Kinetic Parameters of the Wild Type and Thr 342 Mutant Enzymes

			K_d (mM) for	
enzyme	K_m (mg/mL)	k_{cat} (s^{-1})	maltose	α-CD
wild type	1.94 ± 0.20	1280.00 ± 42.3	8.44 ± 0.48	0.75 ± 0.03
T342V	1.84 ± 0.19	98.44 ± 2.50	10.45 ± 0.92	0.21 ± 0.01
T342S	0.39 ± 0.08	3.51 ± 0.32	3.05 ± 0.39	0.19 ± 0.01
T342A	0.26 ± 0.05	0.75 ± 0.01	1.55 ± 0.23	0.34 ± 0.02

RESULTS AND DISCUSSION

Kinetic Parameters of the Thr 342 Mutant Enzymes. The kinetic parameters of the Thr 342 mutant enzymes for amylopectin hydrolysis at 37 °C are summarized in Table 1. The k_{cat} values revealed that all of the Thr 342 mutants were more than 90% inactivated, indicating that this residue may play an important role in the catalytic mechanism. The T342V mutant enzyme showed an approximately 13-fold reduction in enzymatic activity compared to the wild-type enzyme. Despite the decrease in the k_{cat} value of the T342V mutant, there was no significant difference in the K_m value. Replacing the Thr residue with Ser or Ala resulted in even more profound reductions in the enzymatic activity. The k_{cat} values of T342S and T342A were reduced more than 360- and 1700-fold, respectively, compared to that of the wild-type enzyme, indicating that the rate of catalysis was significantly decreased by these mutations. The K_m values of the T342S and T342A mutant enzymes were lower than that of the wild-type enzyme. This is also supported by the fact that the dissociation constants (K_d) of maltose and α-CD from both mutant complexes were also lower than that of the wild-type enzyme (Table 1). Generally, decreased K_m and k_{cat} values indicate that the substrate binds tightly but the catalytic rate is very slow. In this case, the results suggest that even with successful substrate binding at the initial step, the catalysis and product release become much slower. The finding that the decrease of the k_{cat} values (13−1700-fold) was greater than the increase of the K_m values suggested that Thr 342 made a major contribution to catalysis of the SBA or to the productive binding of the substrate.

Quality of the Final Models. Data collection and refinement statistics of each mutant are given in Table 2. The crystals of the apo enzyme and of the T342V/maltose, T342S/maltose, and T342A/maltose complexes diffracted to resolutions of 1.25, 1.12, 1.35, and 1.60 Å, respectively. All crystals belonged to trigonal, $P3_121$, with unit cell dimensions of $a = 84.6-85.1$ Å and $c = 143.1-144.0$ Å. The *R*-factors for the final refined models were 11.79% (R_{free} 15.57%) for the apo enzyme, 11.73% (R_{free} 15.50%) for the T342V/maltose, 11.42% (R_{free} 15.42%) for the T342S/maltose, and 17.08% (R_{free} 20.03%) for the T342A/maltose structures. Ramachandran plots (*22*) obtained for all structural models using the PROCHECK program (*23*) indicated that all residues are in the most favored or additional allowed regions; i.e., there are none in disallowed regions. The root mean square deviations (rmsd) for the Cα coordinates of the apo SBA, T342V/maltose, T342S/maltose, and T342A/maltose with the wild-type/maltose structure (PDB code

Table 2: Data Collection and Refinement Statistics for the Apo Enzyme and Thr 342 Mutant/Maltose Complexes[a]

	apo SBA	T342V/maltose	T342S/maltose	T342A/maltose
diffraction data				
X-ray source	SPring-8 (BL41XU)	SPring-8 (BL38B1)	SPring-8 (BL41XU)	Cu Kα
wavelength (Å)	0.71	0.71	0.71	1.5418
detector	Rigaku R-axis V	ADSC Quantum 4R	Rigaku R-axis V	Bruker Hi-star
crystal system	trigonal	trigonal	trigonal	trigonal
space group	$P3_121$	$P3_121$	$P3_121$	$P3_121$
a, *c* (Å)	84.888, 143.397	84.989, 144.023	85.128, 143.598	84.615, 143.109
resolution limit (Å)	50−1.25 (1.29−1.25)	50−1.12 (1.16−1.12)	50−1.35 (1.40−1.35)	41−1.60 (1657−1.600)
measured reflections	866164 (86076)	902446 (33201)	509264 (49703)	309465 (29740)
unique reflections	163644 (16320)	216884 (13370)	131355 (13026)	76986 (7398)
completeness (%)	99.0 (100.0)	94.4 (58.7)	99.3 (99.5)	97.58 (99.1)
R_{merge}, R_{sym}[b] (%)	6.8 (36.4)	7.3 (40.0)	6.6 (45.5)	6.5 (37.3)
refinement				
program used	SHELXL	SHELXL	SHELXL	CNS
resolution range (Å)	10−1.27 (1.3−1.27)	10−1.28 (1.30−1.28)	10−1.35 (1.40−1.35)	10−1.64 (1.70−1.64)
used reflections	147861 (10059)	144557 (6566)	124411 (12593)	62116 (5606)
completeness (%)	93.82 (95.05)	93.23 (93.88)	94.06 (93.93)	85.2 (77.89)
I/σ	27.8 (7.5)	17.9 (3.7)	18.1 (4.1)	24.7 (5.3)
residues/waters	493/838	493/761	493/906	493/819
sulfate	7	5	6	15
hydrogen	3887	3863	3948	
maltose	0	2	2	2
maltose site		−2 to −1 (α),[c] +1 to +2	−2 to −1 (α/β), (+1) to +2	−2 to −1 (α), +2
average *B*-factor (Å^2)	19.283	17.598	18.023	16.10
bond length rms (Å or deg)	0.014	0.015	0.014	0.0047
bond angle rms	0.030 Å	0.032 Å	0.031 Å	1.255°
R-factor (%)	11.79 (17.7)	11.73 (20.08)	11.49 (24.2)	17.08 (28.62)
R_{free} (%)	15.57	15.50	15.17	20.03 (26.82)

[a] Statistics for the highest resolution shell are given in parentheses. [b] R_{sym} for T342A/maltose. [c] Distorted sugar ring.

1Q6C) were 0.32, 0.14, 0.25, and 0.26 Å, respectively, indicating that these mutations did not induce significant conformational changes. Although the overall structures were almost the same as that of the wild-type/maltose, a striking difference was found at the backbone of residues 340−346 for the T342S/maltose and T342A/maltose structures.

Figure 2 shows the electron density maps for the inner loop of each Thr 342 mutant/maltose complex (black line) superimposed on the wild-type/maltose (yellow line). The backbone structures were well ordered and clearly discernible in all mutant enzymes. The conformation of the main-chain residues 340−346 in the T342V/maltose took the product form and was very similar to that of the wild-type/maltose structure (Figure 2a), while these conformations were clearly different in the T342S/maltose and T342A/maltose structures (Figure 2, panels b and c, respectively). The inner loop in these mutants took the apo form. The aromatic ring of Phe 341 was tilted by rotating the ψ angle by about 40°, and the (ϕ, ψ) angles of residue 342 were (−134.31, −170.85) and (−95.93, −169.49) in the T342S/maltose and T342A/maltose structures, respectively, resulting in an almost 180° rotation of the main-chain O atom of residue 342. Consequently, the Cα atom of the substituted residue 342 moved more than ∼2 Å compared to the wild-type/maltose structure as if it was expelled from the maltose molecules (Figure 2b,c).

Structures of the Wild-Type/Maltose and Each Thr 342 Mutant/Maltose Complex. Figure 3 illustrates the superposition of the wild-type/maltose on each Thr 342 mutant/maltose structure at the active site. In the wild-type/maltose structure, the Thr 342 residue was involved in the hydrogen bonds with both maltose molecules and catalytic acid (Glu 186). The Oγ1 atom of Thr 342 interacted with the Oε2 atom of Glu 186 (2.6 Å) and with the O3 and O4 atoms of Glc(+1) (2.7 and 3.3 Å, respectively). In addition, the carbonyl oxygen of Thr 342 created hydrogen bonds with the O1 atom of Glc(−1) with a distorted sugar ring and the O3 atom of Glc(+1) at respective distances of 3.1 and 3.3 Å.

T342V/Maltose Complex. The inner loop of the T342V/maltose structure took the product form as the wild-type/maltose structure did (Figure 3a). The side chain of Val 342 has no ability to create three hydrogen bonds with the Oε2 atom of the Glu 186 residue or with the Glc(+1) that existed in the wild-type/maltose structure, while the carbonyl oxygen of Val 342 maintained the hydrogen bonds with the Glc(−1) and Glc(+1). Furthermore, there were conformational changes in the side chain of Val 342 and Glu 186. The fact that the T342V mutant enzyme exhibited a 13-fold decrease in activity despite its structural similarity with the wild-type enzyme, especially at its inner loop conformation, indicates the significance of the Oγ1 atom, which has an ability to create hydrogen bonds with Glu 186 and Glc(+1). One of the conceivable roles of the side chain of Thr 342 is to stabilize the deprotonated state of Glu 186 by hydrogen bonding to it after the cleavage of the scissile bond. Simultaneously, the Oγ1 atom of Thr 342 creates the hydrogen bonds to the O4 and O3 of the Glc(+1), which are formed after the cleavage of glycosidic bond atoms and seem to prevent the remaining substrate from the dissociation out of the active site pocket.

T342S/Maltose Complex. The hydrogen bonds formed between Thr 342 and Glu 186, Thr 342 and Glc(−1), and Thr 342 and Glc(+1) were almost lost and were rearranged in the T342S/maltose and T342A/maltose structures due to the alternative conformation of the inner loop, which was reflected in the transition from the product form to the apo form (Figure 3b,c). In the T342S/maltose structure, the Oγ atom of Ser 342 was 2.6 Å from the O1 atom of Glc(−1),

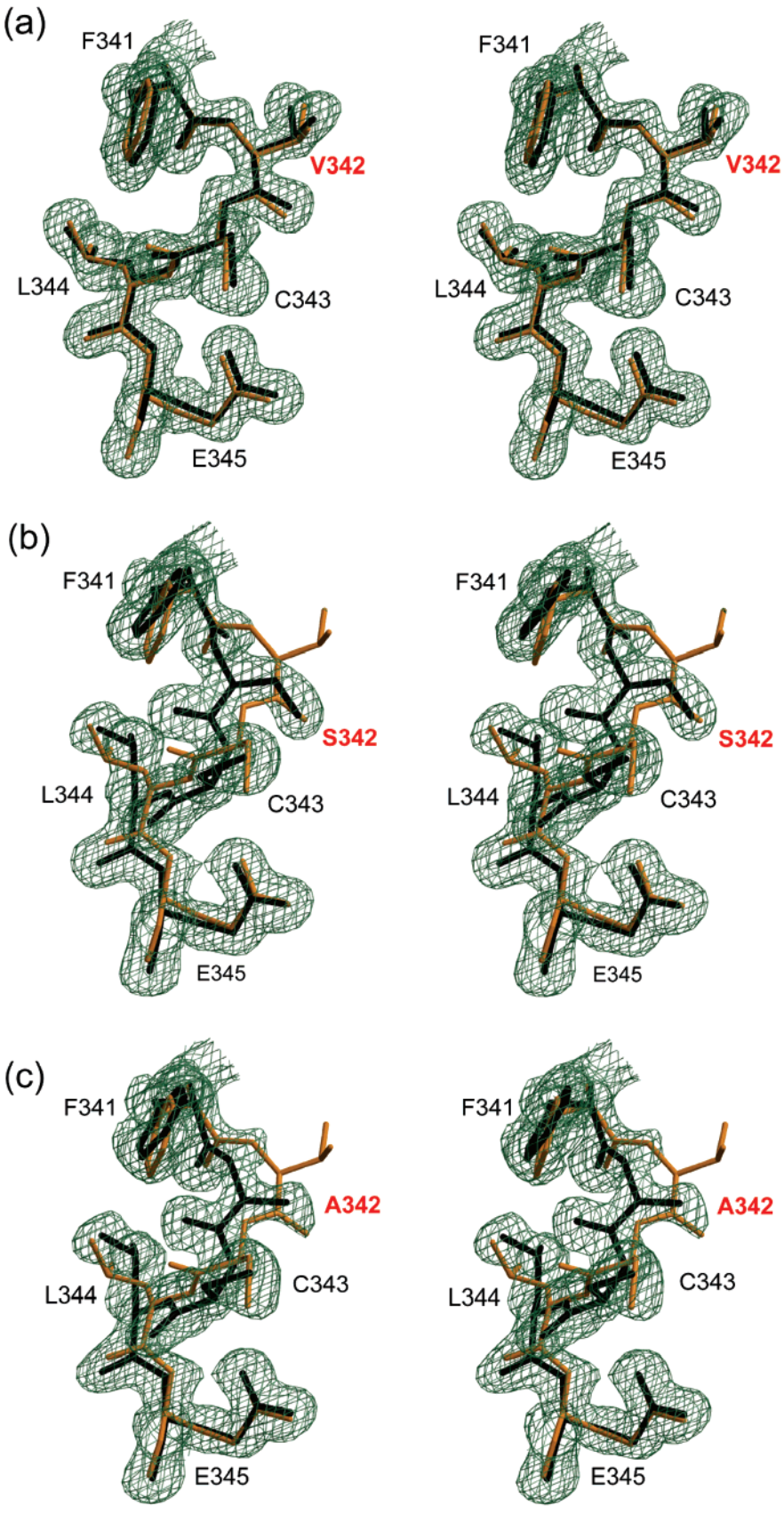

FIGURE 2: Stereoviews of the electron density maps observed for the inner loop of the (a) T342V/maltose, (b) T342S/maltose, and (c) T342A/maltose complexes in comparison with the wild-type/maltose complex. The Thr 342 mutants are indicated by a black line and the wild-type/maltose by a yellow line. Electron densities in $2F_o - F_c$ maps are contoured at 1σ. The backbone structures are well ordered and clearly discernible in all mutant enzymes. The inner loop conformation of the T342V/maltose was very similar to that of the wild-type/maltose complex as the product form, while these conformations were clearly different in the T342S/maltose and T342A/maltose structures as the apo form.

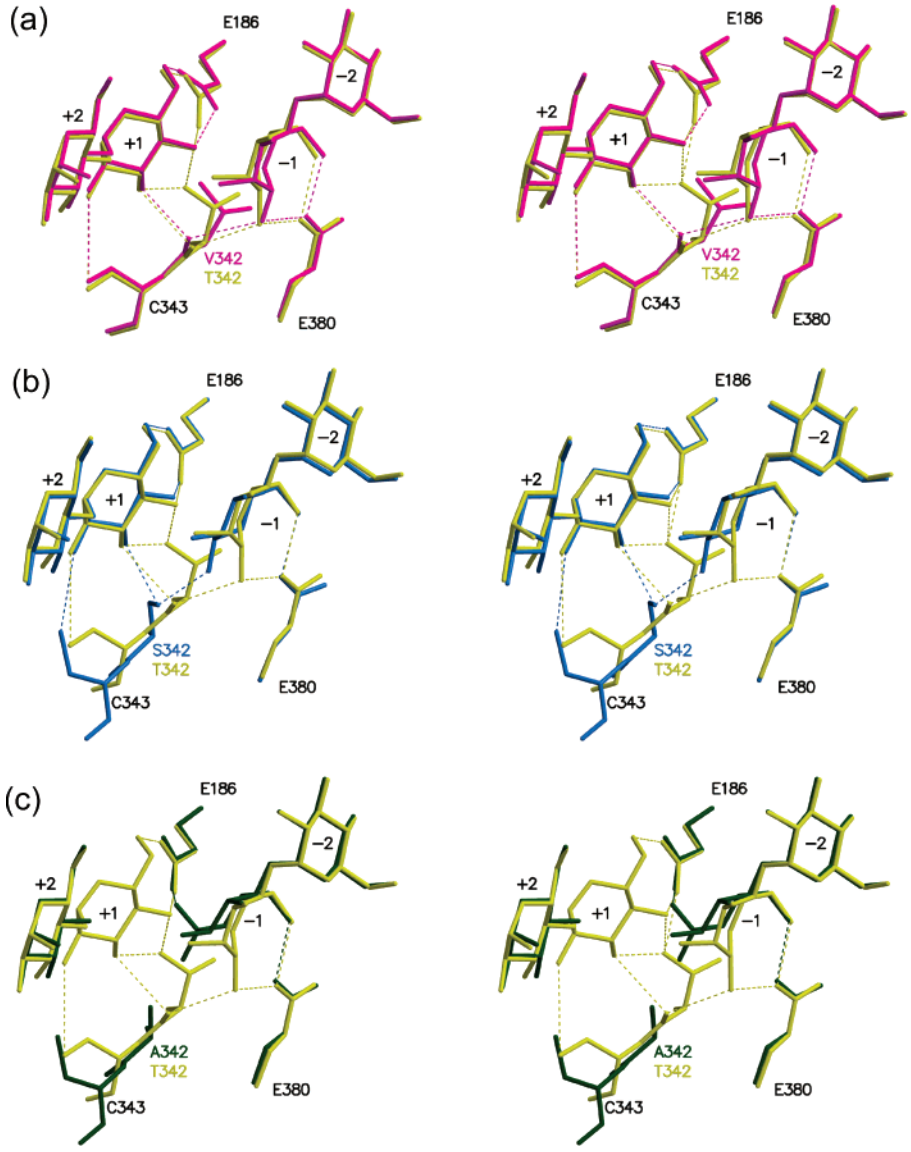

FIGURE 3: Hydrogen-bonding networks of the wild-type/maltose complex (yellow) and each of the Thr 342 mutant/maltose complexes in stereo: (a) T342V/maltose structure (magenta), (b) T342S/maltose structure (blue), and (c) T342A/maltose structure (dark green).

occupying the position corresponding to the carbonyl O atom of Thr 342 in the wild-type enzyme, although the two positions were not exactly identical. Therefore, the hydrogen bond of the O3 atom of Glc(+1) with the O atom of Thr 342 in the wild-type/maltose (3.3 Å) was replaced by the Oγ atom of Ser 342 in T342S/maltose (2.9 Å). On the other hand, the hydrogen bond between the Oγ1 of Thr342 and the Oϵ2 of Glu 186 in the wild-type/maltose complex was broken because the main chain of the Ser 342 residue was in the apo form, and this form could not support the interaction with the Oϵ2 atom of Glu 186.

T342A/Maltose Complex. The Ala 342 in the T342A/maltose structure does not have any significant interactions with Glc(−1) or with Glu 186 (Figure 3c). The Glc(−1) showed a stable $^4C_1$ chair conformation with a mixture of α- and β-anomeric forms at its O1 atom, and this glucose residue was relatively close to the position of the subsite +1 compared to other known structures of SBA/maltose. Moreover, the main-chain conformation of Ala 342 prevented the carbonyl oxygen of Ala 342 from creating a hydrogen bond with the putative attacking water molecule. Consequently, all of the potential stabilizing interactions between Ala 342 and the glucose residues at subsites −1 and +1 which were found in the wild-type/maltose structure were virtually nonexistent in the T342A/maltose structure.

Table 3: Sugar Conformation Parameters Found in Thr 342 Mutants Complexed with Maltose

sugar sites	puckering parameters[a] Φ^2 (deg)	Θ (deg)	Q (Å)	form	anomer (occupancy)
T342V					
−2	0.6217	6.67	142.0369	$^4C_1$	α (1.0)
−1	0.6991	80.04	234.1705	$^{1,4}B$	α (1.0)
+1	0.5686	11.81	273.7215	$^4C_1$	α (1.0)
+2	0.5873	3.52	200.5987	$^4C_1$	α (1.0)
T342S					
−2	0.6302	6.19	177.2078	$^4C_1$	α (1.0)
−1	0.6353	8.51	223.9760	$^4C_1$	α/β (0.3/0.7)
+1	0.6754	14.14	279.6375	$^4C_1$	α (0.7)
+2	0.6018	6.29	229.1679	$^4C_1$	α (1.0)
T342A					
−2	0.5850	4.65	138.2472	$^4C_1$	α (1.0)
−1	0.5740	1.33	47.3334	$^4C_1$	α/β (0.5/0.5)
+2	0.5866	3.43	220.3950	$^4C_1$	α (1.0)

[a] The puckering parameters (Φ^2, Θ, Q) were calculated by the PLATON program (*21*).

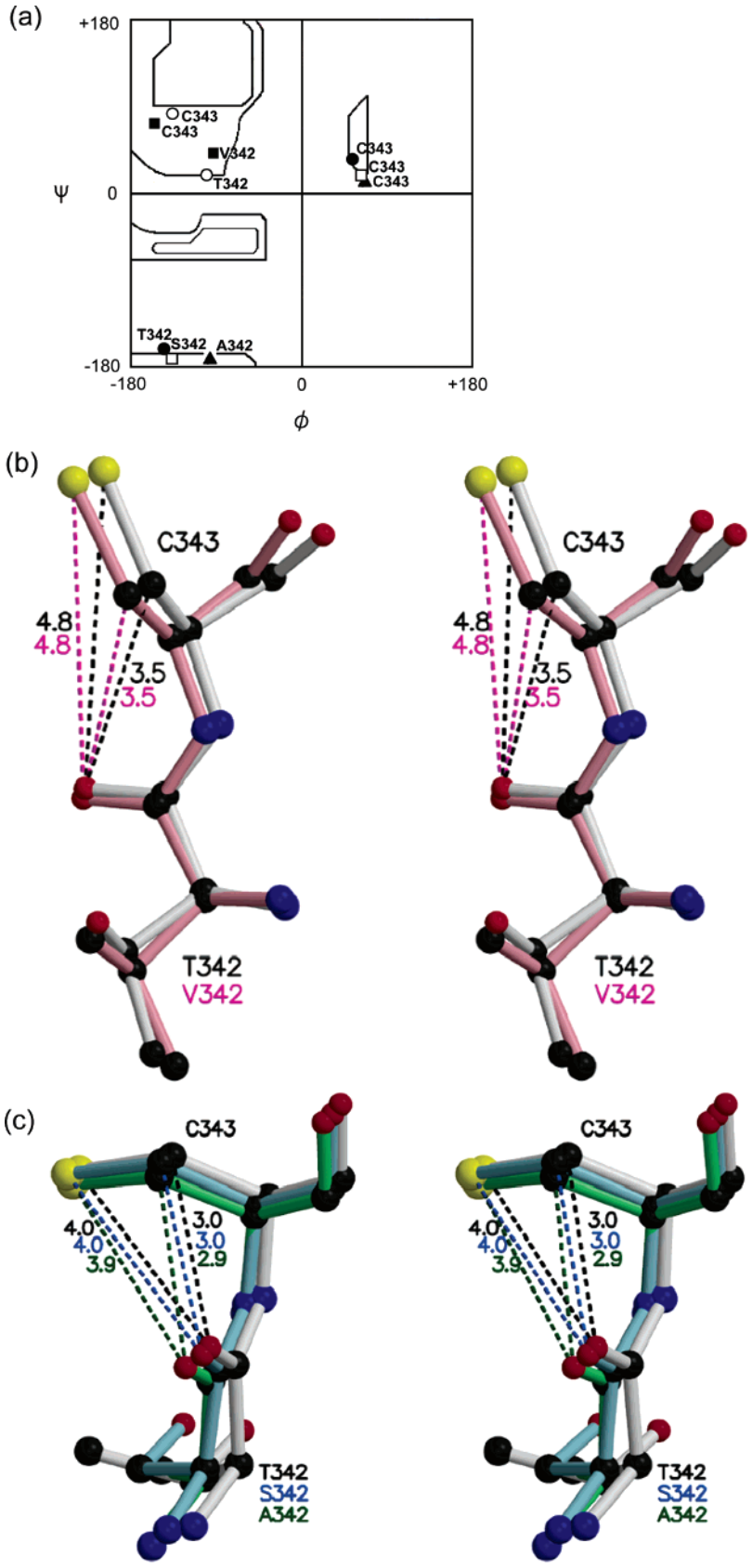

FIGURE 4: (a) The dihedral angles (ϕ, ψ) of residues 342 and 343 on the Ramachandran plot for the apo SBA (●), wild-type/maltose (○), T342V/maltose (■), T342S/maltose (□), and T342A/maltose (▲) structures. The (ϕ, ψ) of Cys 343 in the apo SBA, T342S/maltose, and T342A/maltose structures, whose inner loops adopt the apo form, are in the left-handed helix region, while those of the wild-type/maltose and T342V/maltose structures are in the most favorable region. (b) Distance between the Cβ atom of Cys 343 and the O atom of Thr 342 in each SBA structure. The structures of the wild-type/maltose (gray) and the T342V/maltose (pink) were superimposed at the inner loop (product form) in stereo. (c) Superimposition of the inner loops (apo form) of the apo SBA (gray), T342S/maltose (light blue), and T342A/maltose (light green) in stereo. In the structures whose inner loops adopt the apo form, the distances between the Cβ atom of Cys 343 and the backbone O atom are about 3.0 Å, and these appear to be steric hindrance at those positions.

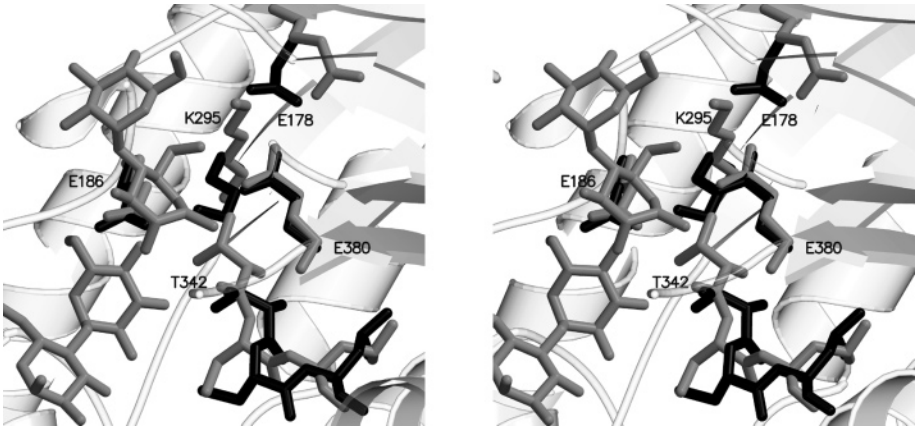

FIGURE 5: Superimposition of the apo enzyme (black) and the wild-type/maltose enzyme (gray) at the active site in stereo. Note that the conformations of the Lys 295, Glu 178, and the inner loop (Thr 342) between these two structures are significantly different.

Bound Sugar Conformations of Each Thr Mutant/Maltose Complex. The bound maltose molecules were found at subsites −2 to −1 and +1 to +2 for the T342V/maltose and T342S/maltose complexes. In the T342A/maltose complex, one maltose was found at subsite −2 to −1 and one glucose residue was found at subsite +2. The different anomers at subsite −1 were revealed by the present higher resolution work. Table 3 shows the puckering parameters of the glucose rings at each subsite. The conformations of the pyranose ring compounds are often described by the puckering parameters (Φ^2, Θ, Q) (*20*). The sugar ring at subsite −1 of the T342V/maltose structure was found to be a distorted ^{1,4}B α-anomer as was found in the wild-type/maltose complex structure, while all of the sugar rings in the T342S/maltose and T342A/maltose complexes showed a stable undistorted $^4C_1$ chair conformation. The configurations of the Glc(−1) in the T342S/maltose and T342A/maltose were found to be mixtures of α/β with an occupancy of 0.3/0.7 and 0.5/0.5, respectively. The glucose residue at subsite −1 with the $^4C_1$ α-anomer in the T342S/maltose and T342A/maltose structures inhibited the sugar binding at subsite +1 due to the steric hindrance between the O1 atom of Glc(−1) and the O4 atom of Glc(+1) as found in the E380Q/maltose (*10*), E178Y/maltose, and N340T/maltose complexes (*24*).

Dihedral Angles of Thr 342 and Cys 343 and Inherent Strain in the Inner Loop. Figure 4a shows the dihedral angles (ϕ, ψ) of residues 342 and 343 on the Ramachandran plot for the apo SBA, wild-type/maltose, and Thr 342 mutant/maltose structures. In the wild-type/maltose and T342V/maltose structures, whose inner loop adopted the product form, the (ϕ, ψ) values of residue 342 were in the β-sheet allowed region: (−97.75, 18.72) for Thr 342 in wild-type/maltose and (−92.34, 40.69) for Val 342 in T342V/maltose. The Cys 343 residues were also in the favorable region in the wild-type/maltose and T342V/maltose, with values of (134.54, 83.18) and (−154.74, 72.91), respectively. However, the (ϕ, ψ) values of residues 342 and 343 in the apo SBA, T342S/maltose, and T342A/maltose structures, the inner loops of which adopt the apo form, shifted to regions different from those of the wild-type/maltose and T342V/maltose structures. The (ϕ, ψ) values of residue 342 in the apo SBA, T342S/maltose, and T342A/maltose structures were (−143.42, −160.73), (−134.31, −170.85), and (−95.93, −169.49), respectively. Moreover, the (ϕ, ψ) values of the Cys 343 residues were in the left-handed helix region: (52.82, 35.98) for the apo SBA, (62.83, 18.15) for the T342S/maltose, and (66.83, 14.55) for the T342A/maltose. It is generally accepted that the non-glycine residues in the left-handed helical regions have unfavorable energies because of the local steric interaction of the backbone atoms with the side-chain Cβ atom (*25*−*28*). The distances between the Cβ atom of Cys 343 and the backbone O atom in these structures are about 3.0 Å (Figure 4b,c), which appears to allow steric interaction at these positions.

Pujadas et al. pointed out that the enthalpic cost of the local conformational transition from apo form to product form that involves the Thr 342 and Cys 343 residues is negative, which is strong evidence that the active site cleft that includes these residues is of a metastable nature (*8*). Although relatively few steric strains associated with energetically unfavorable main-chain ϕ/ψ and non-proline *cis*-peptide bonds are observed in the protein structures, those that do occur are overwhelmingly in the regions of the structures intimately involved in functions such as ligand binding and catalysis (*29*). Considering the main-chain conformation of the inner loop and the enzymatic activity of each mutant enzyme together, we conjecture that the main-chain transition from the apo form to the product form involves the enzymatic functions. The shift of the dihedral angles from the strained conformational region in the apo enzyme to the stable region in the wild-type/maltose structure implies that the strain was released during the catalytic step, and this energy released near the active site seems to facilitate the catalysis of the SBA. The torsion angle strain at the active center of the histidine-containing phosphocarrier protein (HPr) is directly involved in protein function, which facilitates the phosphotransfer reaction by lowering the activation energy barrier (*30*). When the inner loop is in the product form, the Thr 342 residue is stabilized by the hydrogen bonds with Glu 186 (catalytic acid) as well as Glc(−1) and Glc(+1). It is possible that the local steric strain in this region can be released by the conformational change and stabilized by these favorable hydrogen bonds during the catalysis of the enzyme.

Relationship between the Movement of Lys 295 and the Inner Loops. Comparison of the structures of the apo enzyme with the wild-type/maltose and mutants/maltose complexes revealed the relationship between the conformational changes during the catalytic process. In the apo enzyme, the flexible

loop is open and the inner loop always takes an apo form. In addition to the flexible loop and the inner loop, the side chain of Lys 295 changes its conformation between the apo and complex forms with maltose (*5*, *9*, *24*), maltal (*5*), α- and *β*-CD (*4*, *7*), and G5 (*10*). Figure 5 shows the superimposition of the active site of the apo enzyme onto the wild-type/maltose complex. The side chain of Lys 295 in the apo form occupies the position of the side chain of Thr 342 in the product form of the inner loop. The Cϵ of Lys 295 makes a complete collision with the Cγ2 of Thr 342. The Nζ of Lys 295 forms a hydrogen bond with the Oϵ2 of Glu 186 in the apo form (2.79 Å). In the enzyme/maltose complex, however, the side chain of Lys 295 changes its position by rotating the χ1 angle by 96°. The Nζ of Lys 295 migrates about 5.2 Å and then forms a hydrogen bond with Oϵ2 of Glu 380 (2.79 Å) and O6 of Glc(−1) (2.90 Å). The side-chain movement of Lys 295 also caused the side-chain conformational change of Glu 178 to avoid the collision, as pointed out in the structure of BCB (9). Lys 295 seems to be very important not only to activate Glu 380 by lowering its pK_a value to extract a proton from the attacking water molecule (*10*) but also to migrate between acid and base catalysts synchronizing with the enzyme action. It is suggested that the movement of Lys 295 may play an important role in regeneration of the deprotonation of Glu 380 and the protonation of Glu 186 after the catalysis.

The conformational change of Lys 295 is not directly linked to the movement of the inner loop in the complex forms. In the enzyme/substrate (maltose) complex forms so far examined, the side chain of Lys 295 takes the complex form without exception, whereas the inner loops can take the apo or product forms as described above. Thus, we can distinguish four different conformations of the active site components of the flexible loop, inner loop, and the side chain of Lys 295. These conformations are all apo, closed-apo-complex, closed-product-complex, and open-apo(product)-complex forms. The last conformation was found in the structures of the enzyme/*β*-CD and enzyme/α-CD complexes (*4*, *7*). In the "all apo" form, in which the flexible loop is open, the movement of Lys 295 from the complex to the apo form can facilitate the movement of the inner loop from the product form to the apo form to avoid the collision between Lys 295 and Thr 342.

Conformation of the Inner Loop and Its Implications for the Catalytic Mechanism of SBA. Structural analyses of the apo and ligand-complexed SBA have revealed that the main chain of 340−346 undergoes a conformational change at least once during the catalytic step. The wild-type apo enzyme as well as the catalytic site mutant, E186Q/G5 (*10*), and the E380Q/G5 complexes (data not shown) maintained the apo form in this region, strongly suggesting that the transition of this region from apo form to product form does not occur only by the substrate binding. The transition of this region probably occurs during hydrolysis, or after the maltose production, or both, rather than during the substrate binding itself. Hydrogen bonds between the Oγ1 of Thr 342 and the deprotonated Glu 186 as well as the Glc(+1) are formed with this main-chain transition.

The results of the sugar conformation analysis (Table 3) showed that the distortion of Glc(−1) found in the T342V/maltose and wild-type/maltose structures was not found in the mutants of T342S and T342A, suggesting that only the

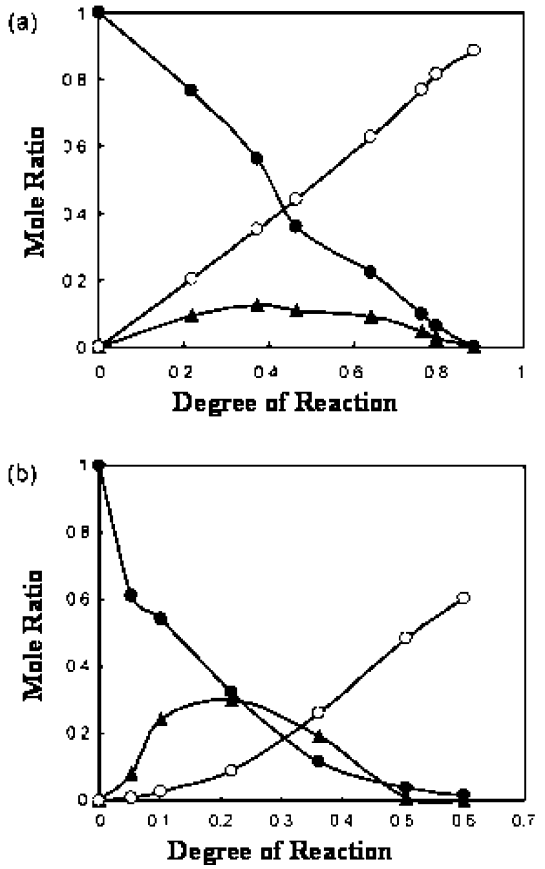

FIGURE 6: Heptamer hydrolysis of (a) wild-type and (b) T342V enzymes. Experimental points are [G7]/[G7]$_0$ (●), [G5]/[G7]$_0$ (▲), and [G3]/[G7]$_0$ (○). The horizontal coordinate shows the degree of reaction defined by the amount of maltose produced. The reactions were carried out with a enzyme concentration of 26.3 nM (a) or 260 nM (b) and [G7]$_0$ = 1.42 mM in 0.1 M sodium acetate buffer, pH 5.5 at 37 °C.

product form with Thr 342 or Val 342 can make the distortion of Glc(−1). In this connection, the Glc(−1) residues found in the E186Q/maltopentaose and E380Q/maltopentaose with the inner loop of the apo form have a $^4C_1$ sugar ring without distortion (*10*). The decreased K_m and K_d values for maltose of the T342S and T342A mutants with the apo form also suggest that one role of the product form of the inner loop is to distort the Glc(−1) sugar ring in order to allow it to accept the hydrolytic attack of the catalytic residues. The lower affinity for maltose in the inner loop with the product form also facilitates the release of the product (Table 1).

Comparison of the protein−ligand interactions between the apo and product forms also suggests that one of the roles of this shift may be to allow grasping of the substrate at subsite +1 after hydrolysis. Bailey and French (*31*, *32*) and recently Nakatani (*13*) have identified the action pattern of *β*-amylase under a variety of conditions using maltodextrins and a synthetic amylose as substrates and confirmed that under all conditions the action pattern was always intermediate between single-chain and multichain, which showed that the enzyme produces several maltose molecules effectively from a single enzyme−substrate complex without dissociation, and thereby allowing the multiple attack mechanism. For the effective hydrolysis of the substrate in SBA, there must be subsite flexibility, and there must be no dissociation of substrate from the active site. The wild-type/*β*-CD

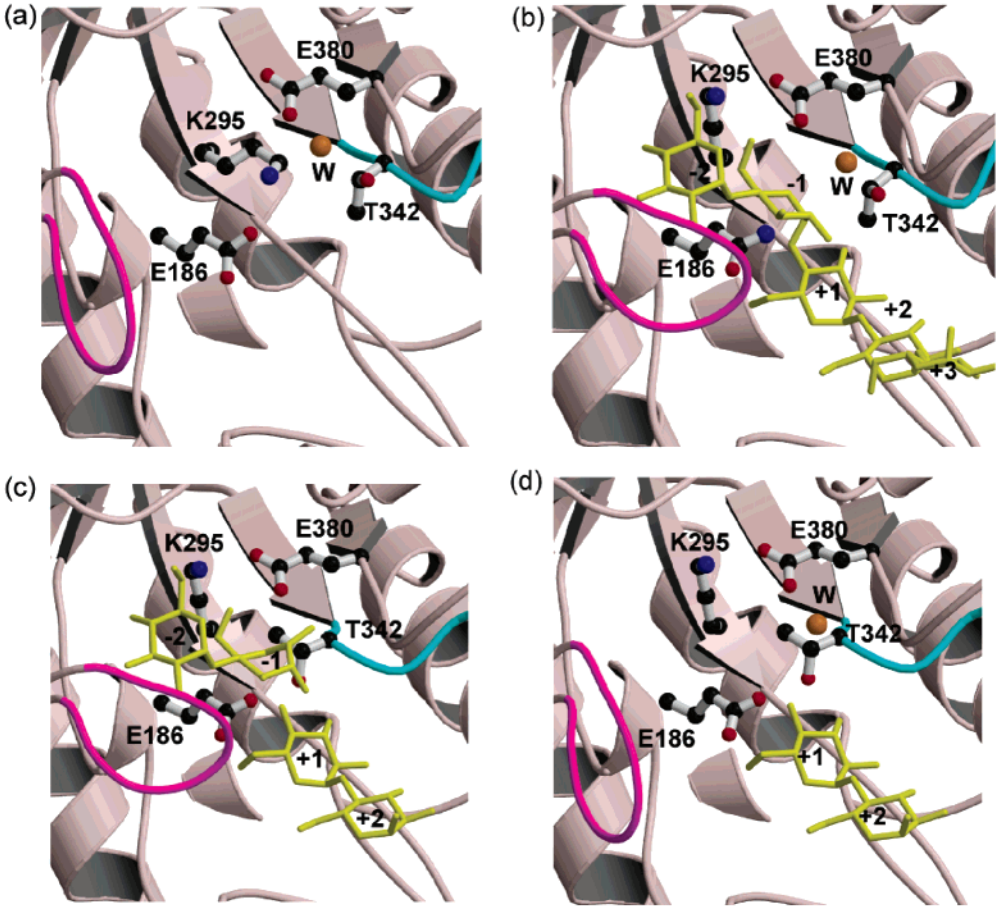

FIGURE 7: Conformations of the flexible loop (96−103) and the inner loop (340−346) at each catalytic step. The flexible loop and inner loop are indicated as a magenta and cyan coil, respectively. Catalytic residues (Glu 186 and Glu 380) as well as Lys 295 are shown in the ball-and-stick model. Sugar rings are represented in yellow. The catalytic water is shown in the orange ball. Panels: (a) apo SBA (PDB code 1WDP); (b) substrate binding (PDB code 1V3H); (c) after cleavage of the scissile bond (PDB code 1Q6C); and (d) after product release, which is estimated from the α-CD complex (PDB code 1BTC) by replacement of α-CD with maltose.

structure has revealed the positional flexibility of glucose binding on subsite +2 and suggested that this may be responsible for substrate slipping (*7*).

To confirm the role of Thr 342 on the multiple attack mechanism of SBA, the time course of product sugars was examined for the wild-type and T342V enzyme using G7 as a substrate (Figure 6). From the amount of G5, which does not appear in the complete single-chain attack, the ratio of single-chain and multichain attacks to the whole reaction was estimated to be 0.5 for the wild-type and 0 for the T342V according to the method of Nakatani (*13*). Though the T342V mutant has enzymatic activity one-tenth that of the wild-type SBA, the result clearly demonstrates the loss of single-chain attack in T342V mutant and supports the view that the side chain of Thr 342 is inevitable for retaining the rest of the substrate on the subsites around +1 to +3 after the release of product.

On the basis of the structural analysis of the apo and Thr 342 mutant/maltose complexes, the following hypothesis can be suggested. The flexible loop and the inner loop adopt the open and the apo forms, respectively, when there is no substrate in the active site (Figure 7a). When the substrate enters into the active site pocket, the flexible loop moves close to the substrate. The substrate-induced closure of this loop covers the active site and fixes the substrate as described previously (*4*, *5*). The side chain of Lys 295 also moved to Glu 380 by the substrate binding, and the inner loop maintained its apo form (Figure 7b). After or simultaneously the scissile bond is cleaved by protonation of Glu 186 to the glycosidic oxygen, and the inner loop springs from its apo form to the product form. At this time, the Thr 342 residue supports the hydrogen bonds to the Glc(−1) and Glc(+1) as well as to the Glu 186 residue. The release of the inherent strain in the main chain of Thr 342 and Cys 343 may facilitate the movement (Figure 7c). The maltose product leaves with the flexible loop of residues 95−103 open, and the substrate at subsites +1 and +2 are held on the active pocket by Thr 342 (Figure 7d). The inner loop returns to the apo form by the conformational change of Lys 295 from complex to apo form. In this step, the rest of the substrate leaves from the enzyme or is retained at subsites higher than +1 and moves to subsites −2 and −1 for the next catalytic step, as the apo form of the inner loop has higher affinity for glucose residues at the subsites than the product form.

ACKNOWLEDGMENT

We thank Drs. M. Kawamoto, H. Sakai, and K. Hasegawa of the Japan Synchrotron Radiation Research Institute (JASRI) for their kind help in data collection. Computation time was provided by the Supercomputer Laboratory, Institute for Chemical Research, Kyoto University.

REFERENCES

1. Henrissat, B. (1991) A classification of glycosyl hydrolases based on amino acid sequence similarities, *Biochem. J. 280*, 309−316.
2. Henrissat, B. (1998) Glycosidase families, *Biochem. Soc. Trans. 26*, 153−156.
3. Thoma, J. A., Spradlin, E., and Dygert, S. (1971) Plant and animal amylases, in *The Enzymes*, 3rd ed., Vol. 5, pp 115−189, Academic Press, New York.
4. Mikami, B., Hehre, J. A., Sato, M., Katsube, Y., Hirose, M., Morita, Y., and Sacchattini, J. S. (1993) The 2.0 Å resolution structure of soybean β-amylase complexed with α-cyclodextrin, *Biochemistry 32*, 6836−6845.
5. Mikami, B., Degano, M., Hehre, E. J., and Sacchettini, J. S. (1994) Crystal structures of soybean β-amylase reacted with β-maltose and maltal: active site components and their apparent roles in catalysis, *Biochemistry 33*, 7779−7787.
6. Davies, G. J., Wilson, K. S., and Henrissat, B. (1997) Nomenclature for sugar-binding subsites in glycosyl hydrolases, *Biochem. J. 321*, 557−559.
7. Adachi, M., Mikami, B., Katsube, T., and Utsumi, S. (1998) Crystal structure of recombinant soybean β-amylase complexed with β-cyclodextrin, *J. Biol. Chem. 273*, 19859−19865.
8. Pujadas, G., and Palau, J. (1997) Anatomy of a conformational transition of β-strand 6 in soybean β-amylase caused by substrate (or inhibitor) binding to the catalytical site, *Protein Sci. 6*, 2409−2417.
9. Mikami, B., Adachi, M., Kage, T., Sarikaya, E., Nanmori, T., Shinke, R., and Utsumi, S. (1999) Structure of raw starch-digesting *Bacillus cereus* β-amylase complexed with maltose, *Biochemistry 38*, 7050−7061.
10. Kang, Y. N., Adachi, M., Utsumi, S., and Mikami, B. (2004) The roles of Glu186 and Glu380 in the catalytic reaction of soybean β-amylase, *J. Mol. Biol. 339*, 1129−1140.
11. Bernfeld, P. (1955) Amylase, alpha and beta, in *Methods in Enzymology*, Vol. 1, pp 149−150, Academic Press, New York.
12. Morita, Y., Yagi, F., Aibara, S., and Yamashita, H. (1976) Chemical composition and properties of soybean β-amylase, *J. Biochem. (Tokyo) 79*, 591−603.
13. Nakatani, H. (1997) Monte Carlo simulation of multiple attack mechanism of β-amylase-catalyzed reaction, *Biopolymers 42*, 831−836.
14. Otwinowski, Z., and Minor, W. (1997) Processing of x-ray diffraction data collected in oscillation mode, *Methods Enzymol. 276*, 307−326.
15. Brünger, A. T., Adams, P. D., Clore, G. M., DeLano, W. L., Gros, P., Grosse-Kunstleve, R. W., Jiang, J. S., Kuszewski, J., Nilges, M., Pannu, N. S., Read, R. J., Rice, L. M., Simonson, T., and Warren, G. L. (1998) Crystallography and NMR system: A new software suite for macromolecular structure determination, *Acta Crystallogr., Sect. D: Biol. Crystallogr. 54*, 905−921.
16. Sheldrick, G. M. (1997) SHELX-97, a Program for the Refinement of Single-Crystal Diffraction Data, University of Gottingen, Gottingen, Germany.
17. Kraulis, P. J. (1997) *MOLSCRIPT*: a program to produce both detailed and schematic plots of protein structures, *J. Appl. Crystallogr. 24*, 946−950.
18. Esnouf, R. M. (1997) An extensively modified version of MolScript that includes greatly enhanced coloring capabilities, *J. Mol. Graphics Modell. 15*, 132−134.
19. Merritt, E. A., and Cacon, D. J. (1997) "Raster3D: Photorealistic Molecular Graphics", *Methods Enzymol. 277*, 505−524.
20. Cremer, D., and Pople, J. A. (1975) General definition of ring puckering coordinates, *J. Am. Chem. Soc. 97*, 1354−1358.
21. Spek, A. L. (2003) Single-crystal structure validation with the program PLATON, *J. Appl. Crystallogr. 36*, 7−13.
22. Ramachandran, G. N., Ramakrishnan, C., and Sasisekharan, V. (1963) Stereochemistry of polypeptide chain configurations, *J. Mol. Biol. 7*, 95−99.
23. Laskowski, R. A., MacArthur, M. W., Moss, D. S., and Thornton, J. M. (1993) PROCHECK: a program to check the stereochemical quality of protein structures, *J. Appl. Crystallogr. 26*, 283−291.
24. Hirata, A., Adachi, M., Sekine, A., Kang, Y. N., Utsumi, S., and Mikami, B. (2003) Structural and enzymatic analysis of soybean β-amylase mutants with increased pH optimum, *J. Biol. Chem. 279*, 7287−7295.
25. Nicholson, H., Soderlind, E., Tronrud, D. E., and Matthews, B. W. (1989) Contributions of left-handed helical residues to the structure and stability of bacteriophage T4 lysozyme, *J. Mol. Biol. 210*, 181−193.
26. Eswar, N., and Ramakrishnan, C. (1991) *Perspectives in structural biology*, pp 181−195, Indian Academy of Science, Bangalore, India.
27. Gibrat, J. F., Robson, B., and Garnier, J. (1991) Influence of the local amino acid sequence upon the zones of the torsional angles phi and psi adopted by residues in proteins, *Biochemistry 30*, 1578−1586.
28. Stites, W. E., Meeker, A. K., and Shortle, D. (1994) Evidence for strained interactions between side-chains and the polypeptide backbone, *J. Mol. Biol. 235*, 27−32.
29. Herzberg, O., and Moult, J. (1991) Analysis of the steric strain in the polypeptide backbone of protein molecules, *Proteins 11*, 223−229.
30. Jia, Z., Vandonselaar, M., Quail, J. W., and Delbaere, L. T. (1993) Active-centre torsion-angle strain revealed in 1.6 Å-resolution structure of histidine-containing phosphocarrier protein, *Nature 361*, 94−97.
31. Bailey, J. M., and French, D. (1957) The significance of multiple reactions in enzyme-polymer systems, *J. Biol. Chem. 226*, 1−14.
32. French, D. (1961) Action pattern of β-amylase, *Nature 190*, 445−446.
33. Jeannmougin, F., Thompson, J. D., Gouy, M., Higgins, D. G., and Gibson, T. J. (1998) Multiple sequence alignment with ClustalX, *Trends Biochem. Sci. 23*, 403−405.

BI0476580